Controlling Frost Propagation on Polymeric Surfaces Using SI-ATRP Chemical Micropatterning

Tavaststjerna, Miisa J.; Picken, Stephen J.; Garcia, Santiago J.

DOI
10.1002/admi.202400838

Publication date
2025

Document Version
Final published version

Published in
Advanced Materials Interfaces

ADVANCED MATERIALS INTERFACES
Open Access
www.advmatinterfaces.de

Controlling Frost Propagation on Polymeric Surfaces Using SI-ATRP Chemical Micropatterning

Miisa J. Tavaststjerna, Stephen J. Picken, and Santiago J. Garcia*

Micropatterned surfaces with both hydrophilic and hydrophobic regions are relevant for a wide range of applications from fuel cells to water harvesting systems. The preferential nucleation of water on hydrophilic regions can also be used to control frost nucleation on chemically patterned surfaces. So far, this concept has been tested on brittle silicon surfaces with only a few different sizes and shapes of hydrophilic regions. In this work, the concept of controlled icing is investigated on five polymeric surfaces with different surface energies modified by micropatterning them with three types of hydrophilic polymer brushes. Frost formation and propagation on the resulting patterned surfaces with regions of varying wettability is monitored and quantified using high-resolution thermal imaging. The study proves that control over frost nucleation and propagation using regions of varying wettability can be achieved on commodity polymers. In addition to influencing the time and location of ice nucleation, the local patterning affects the freezing propagation mode and rate due to its impact on the continuity and thickness of molecular water layers (MWL). These results show that local control over the state of MWLs is key to controlling both ice nucleation and propagation of freezing events on surfaces.

1. Introduction

To combat ice accretion on surfaces, two strategies have received most of the attention: i) the development of active deicing systems and ii) the fabrication of passive low ice-adhesion surfaces.[1–3] Unfortunately, these strategies have intrinsic disadvantages and are often combined to be able to reach good performance in real-life applications.[4–5] A less explored alternative, is to influence ice nucleation and growth.[6–7] In this strategy, instead of removing already accreted ice from surfaces, surfaces could be fabricated to direct ice growth toward the formation of brittle ice structures that can be continuously removed by environmental factors, such as wind, of relevance in applications as wind turbines, electric cables, and airplanes.

The first step toward controlling ice formation is to gain a better understanding of the early freezing mechanisms at surfaces and to investigate them at a molecular level. In this regard, it is important to consider the role of adsorbed interfacial water in the initial nucleation events. The presence of submicron molecular water layers (MWL) has been reported on all dry surfaces as long as there is some humidity in the environment. However, its state varies in continuity and thickness depending on the surface wettability and environmental conditions.[8–17] In general, the MWL thickness and continuity increase with higher hydrophilicity of the surface (lower water contact angle) and higher environmental humidity.

In our previous work, we connected the presence and state of MWL to various freezing events observed on smooth functionalized glass surfaces via high-resolution thermal imaging.[17] The presence of solid-like MWL was found to promote the speed of inter-droplet ice bridging and deposition frost growth, whereas, very hydrophilic surfaces at high humidity showed rapid freezing propagation via a continuous liquid-like MWL. Since MWLs clearly affect the type and rate of freezing propagation on surfaces,[17] spatial control over the state and thickness of MWLs may also lead to localized control over freezing mechanisms on surfaces with both hydrophilic and hydrophobic regions.

Even though surfaces with wettability patterns, also known as contrast wettability surfaces, have been a popular topic among researchers working on water-harvesting applications[18–23] and microfluidics,[24–27] there are very few studies investigating their effect on freezing.[28–33] In one of the first reports, the spatial control of water condensation and freezing was observed using fluorinated silicon (Si) micropillars with hydrophilic polyvinyl alcohol tips.[28] When the samples were cooled to −15 °C the water

M. J. Tavaststjerna, S. J. Garcia
Department of Aerospace Structures and Materials
Faculty of Aerospace Engineering
Delft University of Technology
Kluyverweg 1, Delft 2629 HS, The Netherlands
E-mail: M.J.Tavaststjerna@tudelft.nl
S. J. Picken
Department of Chemical Engineering
Faculty of Applied Sciences
Delft University of Technology
Van der Maasweg 9, Delft 2629 HZ, The Netherlands

The ORCID identification number(s) for the author(s) of this article can be found under https://doi.org/10.1002/admi.202400838

DOI: 10.1002/admi.202400838

droplets froze one by one via ice-bridge formation on the hydrophilic tips of the pillars. Similar freezing propagation based on ice-bridging was also reported on smooth fluorinated Si surfaces with hydrophilic silicon oxide micropatterning.[30] A follow-up study using the same smooth patterned Si surfaces found that introducing ice-nucleating proteins on top of the hydrophilic silicon oxide micropatterns results in the formation of dry zones around frozen hydrophilic regions.[31] The same effect has also been observed on gold substrates patterned with hydrophilic polyelectrolyte brushes in low supersaturation freezing conditions ($S < 1.5$).[32] This phenomenon has been explained by the formation of a humidity sink as described already in 1981 during the investigation of water condensation around salt crystals.[36] Once the hydrophilic areas freeze in low supersaturation conditions, the frozen regions act as humidity sinks and prevent nucleation events on the hydrophobic surrounding areas.[34–39] This is a result of the saturation vapor pressure over ice being slightly lower than over liquid water.[34]

So far, preferential freezing onset and frost growth on patterned wettability surfaces have been successfully presented either on brittle silicon surfaces and/or in low supersaturation environments with reduced nucleation density of condensation.[30–34] However, there is no information on how this phenomenon would work on more durable polymeric surfaces, similar to those encountered in actual applications, and when the environmental conditions fluctuate between high and low supersaturation. There is also a lack of systematic studies on the role of chemistry of the pattern, the size, shape, or distribution of the hydrophilic regions, and how changes in these parameters influence the type of frost or ice accretion on the surfaces.

To address the aspects above, in this work, we create polymeric surfaces with patterned wettability by modifying various hydrophobic polymeric substrates with three different hydrophilic polymer brushes. The effect of the substrate (local) wettability and the pattern chemistry on the freezing onset and propagation is investigated in a high supersaturation environment ($S > 6.5$) using a digital microscope and high-resolution thermal imaging.

2. Results and Discussion

2.1. Preparation of Patterned and Nonpatterned Surfaces

To investigate systematically the effect of patterned wettability on freezing onset and propagation on the hydrophilic/hydrophobic surfaces, five different polymeric substrates were grafted with three different hydrophilic polymer brushes. The polymeric substrates used in this study are polycarbonate (PC), polypropylene (PP), poly(methyl methacrylate) (PMMA), polyvinylchloride (PVC), and polyurethane (PU). The polymeric brushes were linked covalently to the substrates using a bifunctional macroinitiator (PAzBrMA). **Figure 1** shows the chemical structures of the PAzBrMA and the three hydrophilic polymer brushes used in this study. The synthesis of PAzBrMA consisted of a reversible addition-fragmentation chain-transfer (RAFT) polymerization of glycidyl methacrylate (GMA),[40–42] a ring-opening reaction between the epoxide groups of the poly(glycidyl methacrylate) (PGMA) and sodium azide (NaN_3),[43–44] and an esterification reaction between the OH-groups of the azide-functional polymer (PAzMA) and 2-bromoisobutyryl bromide (BIBB)[44–45] (see Figure S1 in the Supporting Information).

To obtain the functionalized polymeric substrates, as visualized in **Figure 2**, sample preparation started with spin-coating PAzBrMA (10 mg mL^{-1}) on each polymer surface (PC, PP, PMMA, PU, and PVC). After spin-coating, the surface was exposed to UV light (<400 nm, 5 min) which initiated a reaction between the azide groups of the PAzBrMA and the hydrocarbon chain of the polymeric substrates, thus covalently linking the macroinitiator to the polymer surface.[45] To remove any unreacted PAzBrMA, the samples were rinsed with Ethanol-Acetone (6:1) mixture and dried under nitrogen flow (Figure 2, step 3). When a striped mask (100 µm wide stripes with 0.5 mm spacing) was covering the surface during the UV exposure, only the areas exposed to UV allowed for the fixation of PAzBrMA on the surface; rinsing removed then the unreacted PAzBrMA at the areas covered by the mask and not exposed to UV light (Figure 2, step 2 –left). In the last step of sample preparation, the areas functionalized with PAzBrMA were rendered hydrophilic via surface-initiated atom transfer radical polymerization (SI-ATRP) of the monomers 2-hydroxyethyl methacrylate (HEMA), 2-(dimethylamino)ethyl methacrylate (DMAEMA), or poly(ethyleneglycol) methacrylate (PEGMA) followed by washing (Figure 2, steps 4–5). Similar to the azide groups attaching PAzBrMA to the sample surfaces, the bromide functionalities (Br) were used as initiation points for the surface-initiated polymerization of the polymer brushes on the (patterned) surfaces.[45–47]

To confirm patterning, fourier transform infrared spectroscopy (FTIR) and optical microscopy analysis were performed. As a representative example, **Figure 3** shows a confocal scanning microscopy (CSM) and micro-FTIR images of a PHEMA stripe on PP. The thickness of the stripes was measured to be ≈200 nm as seen in the roughness profile of the stripe in Figure 3c. The successful functionalization at the optically detectable patterns with the intended chemical groups was confirmed using micro-FTIR by mapping the absorbance intensity of C═O vibration at 1720 cm^{-1} as seen in Figure 3b.

2.2. Surface Wettability and Roughness

To assess the wettability of the patterned hydrophilic /hydrophobic surfaces, water contact angle measurements were conducted on all bare polymeric substrates and the substrates fully covered with the hydrophilic polymer grafts (i.e., no patterns). **Figure 4a** shows the static (S-WCA), advancing (A-WCA), and receding water contact angles (R-WCA) on all bare polymer substrates (PC, PP, PMMA, PVC, and PU), as well as their water contact angle hysteresis (CAH). The S-WCAs of the substrates vary between 77° and 104°, PP having the highest and PMMA the lowest S-WCA of the polymers. The substrates vary particularly in their CAH values, with PC having the lowest CAH at 25° and PU the highest CAH at 74°. The roughness values of the bare substrates (Figure 4b) follow a similar trend as the CAH values, with PC having the lowest mean area roughness (S_a = 0.06 µm) and PU having the highest S_a (S_a = 0.5 µm).

As seen in Figure 4c, after the surface grafting, the S-WCAs of the PDMAEMA, PHEMA, and PPEGMA-covered substrates

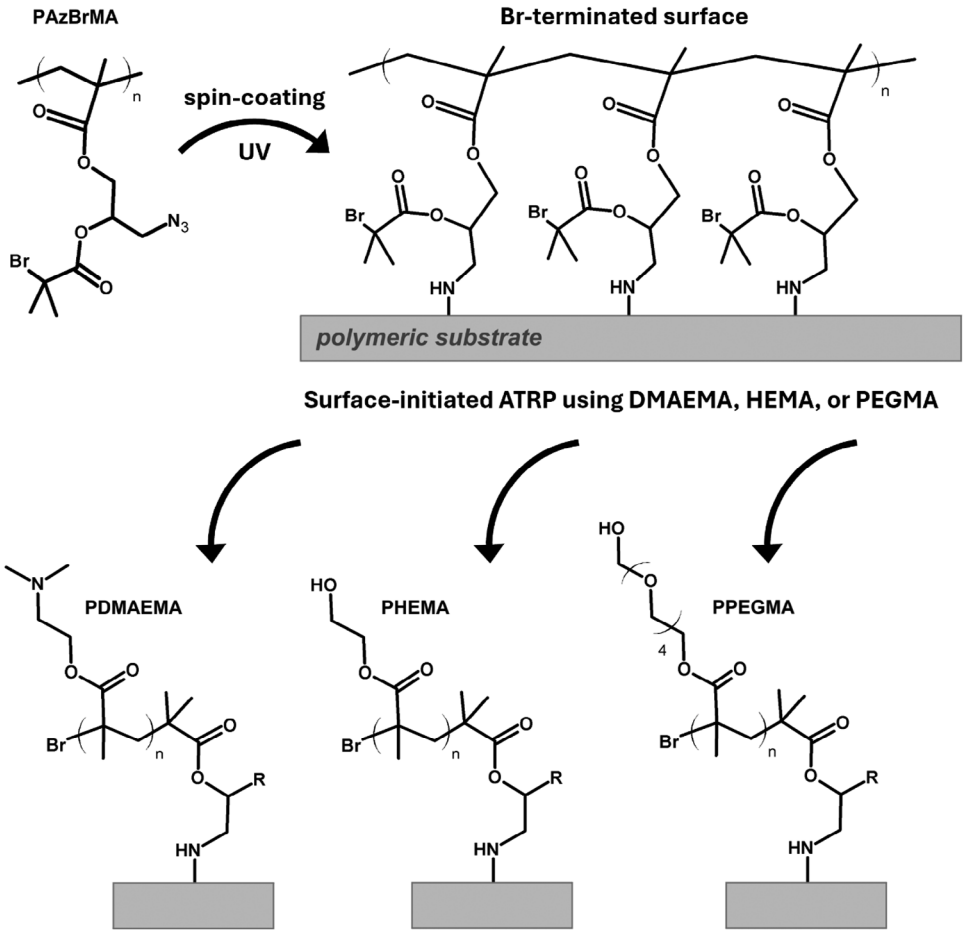

Figure 1. Chemical structures of the bifunctional macroinitiator poly[3-azido-2-(2-bromo-2-methylpropanoyloxy)propyl methacrylate] (PAzBrMA), and the three polymer brush structures poly[2-(dimethylamino)ethyl methacrylate] (PDMAEMA), poly(2-hydroxyethyl methacrylate) (PHEMA), and poly[poly(ethylene glycol) methacrylate] (PPEGMA).

decreased from 77° to 104° corresponding to the substrate polymers to 53°, 41°, and 26°, respectively. Since all the fully grafted surfaces were characteristically hydrophilic, all their R-WCAs are 0°, thus making their CAH values practically equal to their S-WCAs. Additionally, the underlying polymeric substrates did not seem to affect the wettability of grafted samples, confirming a homogeneous surface coverage with hydrophilic polymer grafts. The roughness values of the hydrophilic surfaces, as represented in Figure 4d for the case of PP and PU substrates, are similar regardless of the chemistry of the polymeric graft. Since the thickness of the polymer grafting is ≈200 nm (Figure 3c) the overall roughness values of the hydrophilic samples did not change significantly compared to the bare polymeric substrates.

2.3. Frost Propagation on Nonpatterned Polymer Substrates

To investigate the freezing onset and propagation on homogeneous surfaces, the nonpatterned polymeric samples were cooled to −20 °C at a rate of 8 °C min^{-1} using a liquid-cooled Peltier plate inside an environmental chamber at RH 50%. The polymer surfaces were monitored during the cooling and freezing propagation experiment from above with a high-resolution thermal camera. In this experiment, thermal imaging reveals the latent heat release during the freezing of supercooled surface water. In practice, this allows following the freezing propagation front throughout the surface with high spatial and temporal resolution once a freezing event starts somewhere on the sample surface.

Figure 5 shows selected snapshots from the thermal videos representative of the freezing propagation on the five different bare polymeric substrates and one PHEMA-grafted PMMA substrate. Example videos of the different samples can be found in Videos S1, S2, S3 (Supporting Information). In the video snapshots, the dark purple color corresponds to a lower temperature, and the bright yellow to a higher temperature. As liquid condensation freezes on the sample surface, a sudden temperature increase (local yellow color in the snapshots) pinpoints the location of the freezing event. Thus, the front line of the freezing propagation on the bare polymeric substrates in Figure 5 can be detected as a rim of bright yellow dots corresponding to the freezing of condensed water droplets on the sample surfaces. The white arrows indicate the direction of the freezing front-line

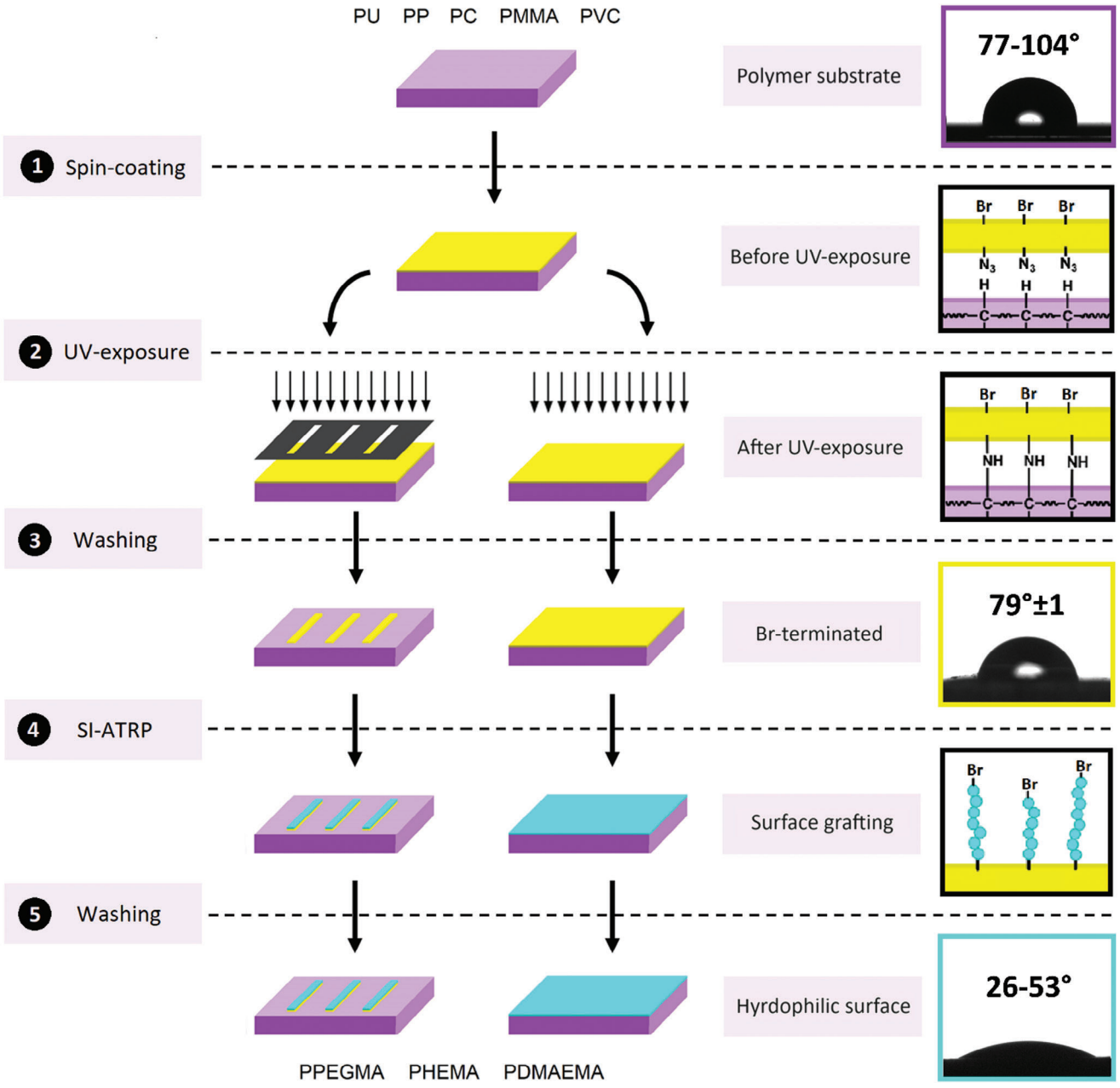

Figure 2. Step-wise representation of the patterned and nonpatterned samples preparation: 1) The polymer substrate (purple) is spin-coated with a solution of PAzBrMA (yellow). 2) UV light attaches the PAzBrMA covalently to the substrate through the azide group. 3) The UV-exposed substrate is rinsed to remove all unreacted PAzBrMA. If a striped mask is used during UV exposure, only the exposed areas are attached to the polymer substrate. 4) The Br-terminated surface is grafted with a hydrophilic polymer (blue) via SI-ATRP. 5) The grafted substrate is removed from the reaction flask, cleaned, and dried before confirming surface modification through contact angle and IR.

propagation. In Figure 5, the freezing propagation front lines on the (slightly)hydrophobic nonpatterned polymeric substrates (WCA>80°) are composed of condensed water droplets individually and sequentially freezing (see Video S1, Supporting Information). A closer examination of the video snapshots reveals small ice bridges interconnecting the frozen droplets (Figure S8 in the Supporting Information). This is in good agreement with an ice-bridging process driving the freezing propagation as reported for percolation-induced frost formation.[48–49]

Freezing onset and propagation rates were also monitored for the substrates fully covered with the hydrophilic PHEMA grafting. The last row in Figure 5 shows one example of the freezing front propagation on the hydrophilic surfaces. In this case, the freezing propagation is captured as a bright yellow rapid wave that eventually fills the entire window of observation. This propagation mode was similar for all the PHEMA-grafted polymeric surfaces, independent of the underlying polymeric substrate (Figure S4 in the Supporting Information). Based on our

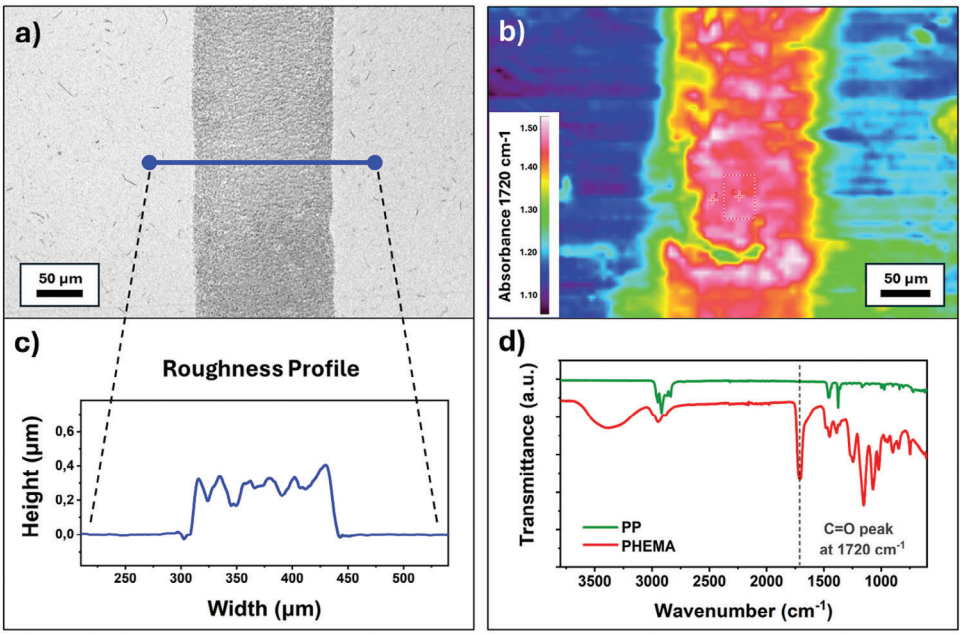

Figure 3. Representative images of patterning for the case of PHEMA stripes on a PP substrate using: a) Confocal Scanning Microscope and b) Micro-FTIR imaging. Roughness profile of the PHEMA stripe c) extracted from the CSM image shows the thickness of the stripe to be ≈200 nm. The red color in the micro-FTIR image visualizes the presence of carbonyl groups present in the repeating unit of PHEMA as shown in the corresponding FTIR spectra d) and the C═O vibrational peak at 1720 cm^{-1}.

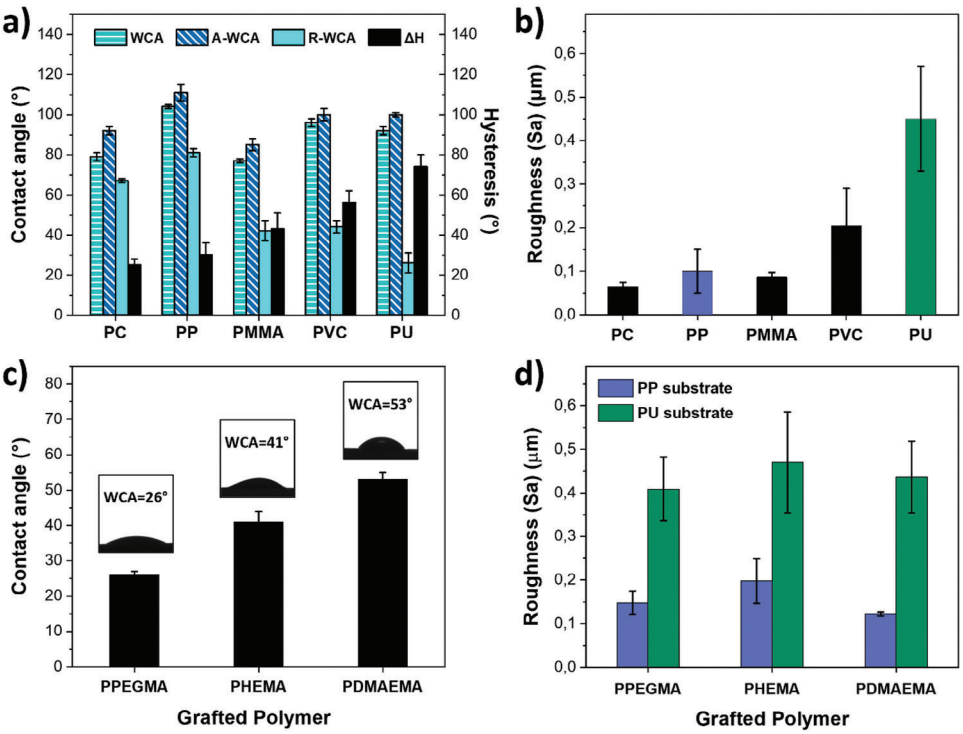

Figure 4. Water contact angle (S-WCA, A-WCA, R-WCA, and CAH) and roughness (S_a) values of the bare substrates a,b) and the samples fully covered with a hydrophilic graft c,d). The static contact angle of substrates coated with hydrophilic grafts (PPEGMA, PHEMA, PDMAEMA) shown in 4c did not depend on the substrate used (PC, PP, PMMA, PVC, PU). The hydrophilic surface grafting also did not significantly influence the roughness of the different polymeric substrates as shown by the consistently different S_a values of PP (blue color) and PU (green color) before b) and after grafting d).

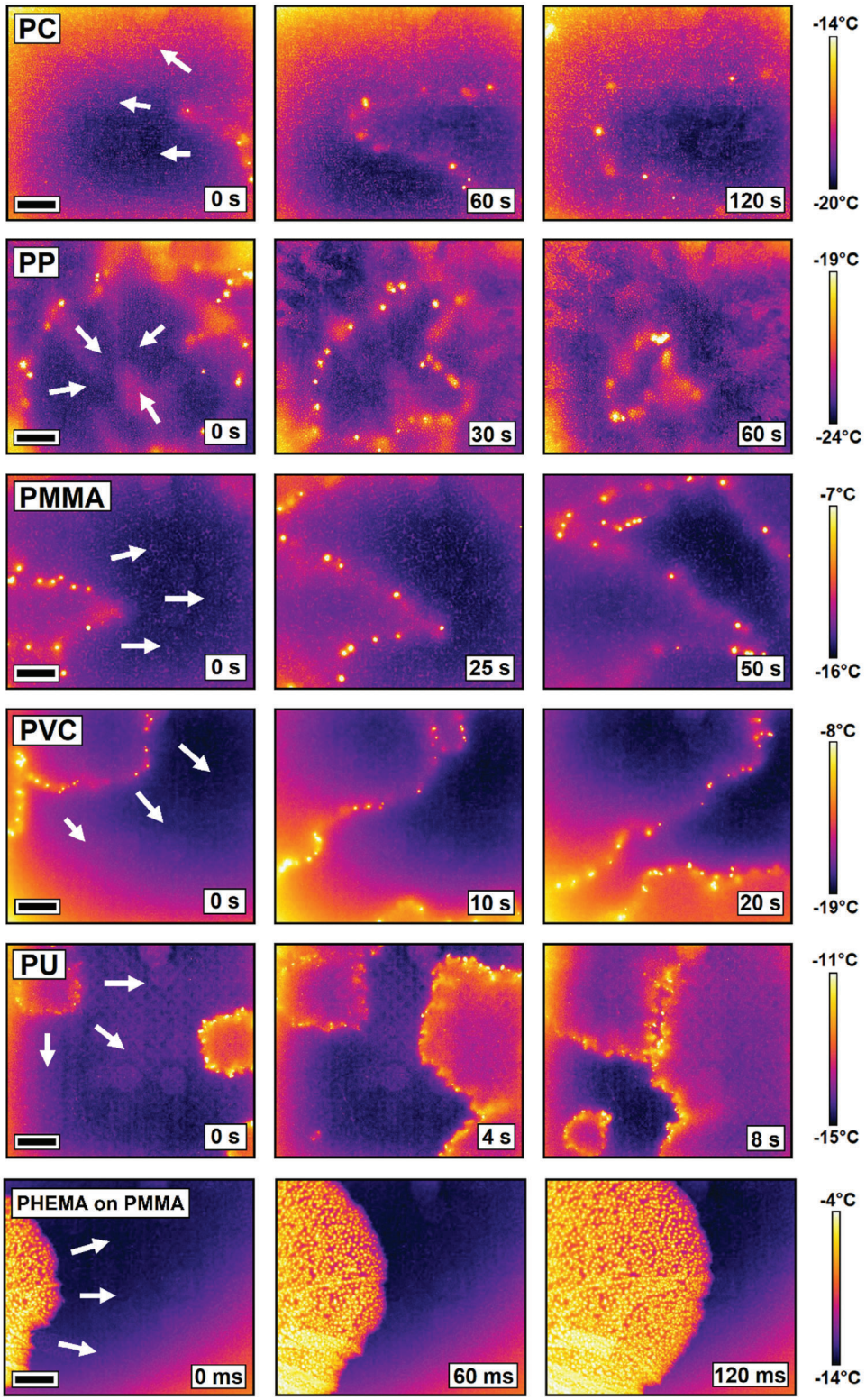

Figure 5. Thermal video snapshots showing freezing propagation on the five nonpatterned polymer substrates (PC, PP, PMMA, PVC, PU) and one PHEMA-grafted PMMA substrate (PHEMA) in RH 50%. The white arrows indicate the direction of the freezing propagation frontline. The black scale bars in the first column of images correspond to 2 mm. Note the time scale for the PHEMA-PMMA sample is in ms (three orders of magnitude faster than the rest of the polymers).

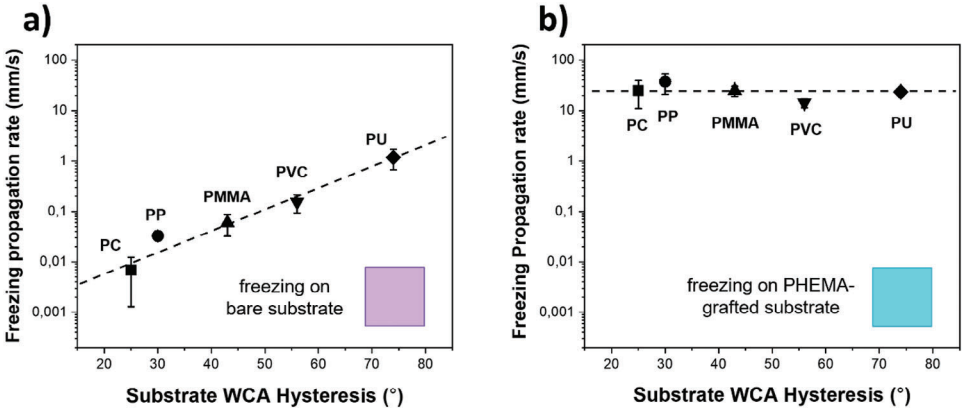

Figure 6. Calculated freezing propagation rates of a) the bare polymers plotted as a function of the substrate CAH; and b) the PHEMA-grafted surfaces plotted as a function of the underlying bare substrate CAH. The same *x*-axis is used in both graphs to highlight the independence of the PHEMA freezing propagation rate from the underlying substrate type.

previous work[17] connecting the presence and state of molecular water layer (MWL) to various freezing events observed on smooth functionalized glass surfaces, the extremely fast freezing frontlines are consistent with freezing events that propagate via a continuous liquid-like MWL.

The thermal snapshots like those shown in Figure 5 were analyzed using the image processing program ImageJ to obtain freezing propagation rates as shown in Figure S7 in the Supporting Information. The average freezing propagation rates with error bars obtained for all nonpatterned samples are shown in **Figure 6** as a function of the substrate WCA hysteresis (CAH).

Despite showing a propagation pattern corresponding to percolation-induced freezing, the measured average propagation rates of the hydrophobic samples (Figure 6a) are significantly higher (between 0.03 mm s^{-1} for PP and 1.2 mm s^{-1} for PU) than those propagation rates previously reported for interdroplet ice bridging characteristic of percolation-induced freezing (0.001–0.01 mm s^{-1}.[48–54]), with the exception of the PC sample (0.007 mm s^{-1}). The results reported here (Figure 6a) therefore extend the previously reported propagation rates for ice-bridging and show for the first time a linear relation between contact angle hysteresis (CAH) and, to a lower extent surface roughness (Figure 4b), with the propagation rate: the higher the difference between advancing and receding angles (higher CAH) the faster the global freezing propagation rate is.

As seen in Figure 5, and different to the hydrophobic surfaces, the freezing propagation frontline on the hydrophilic PHEMA-grafted polymeric surfaces (Video S2 in the Supporting Information) shows a rapid flash-like freezing propagation (e.g., PHEMA on PP) in the scale of ≈20 mm $^{-1}$s (Figure 6b), regardless of the underlying substrate. The slight variation in the freezing propagation rates results from different degrees of supercooling of the PHEMA-covered substrates at the time of nucleation. The cooling stage was set to reach −20 °C at the start of the experiments, but the initial nucleation event can occur before the sample surface has cooled down to this temperature. Freezing events initiated at slightly higher temperatures (lower degree of supercooling) have a slightly lower freezing propagation rate.

Despite the small deviation between experiments, the freezing propagation rates on the hydrophilic surfaces (≈20 mm s^{-1}) are in good agreement with the reported values for freezing propagation in bulk water (≈1–100 mm s^{-1})[55–58] and suggest that the freezing event is propagating through a continuous layer of molecular water layer (MWL). This hypothesis in line with our previous report on MWL-promoted freezing propagation on surface-modified glass[17] and confirms a good homogeneous surface coverage with hydrophilic moieties (e.g., PHEMA) in all cases despite the eventual presence of water droplet freezing.

2.4. Frost Propagation on Patterned Polymer Substrates

Thermal video snapshots of the freezing propagation on the polymer substrates patterned with hydrophilic PHEMA stripes can be seen in **Figure 7** for three polymer substrates (PC, PMMA, PU) and in Figures S5, S6 in the Supporting Information. In all cases the freezing events initiate at the hydrophilic stripes as seen by the 0 ms snapshots, to rapidly propagate longitudinally along the PHEMA stripes (MWL freezing controlled). Once the PHEMA stripes are frozen, the freezing propagation continues laterally outbound from the frozen stripe with the familiar, yellow-dotted front line, highlighting individually freezing of condensed water droplets (interdroplet freezing controlled process).

To study the effect of the hydrophilic stripe chemistry on the freezing onset and propagation, freezing propagation tests on PP substrates with PHEMA, PDMAEMA, or PPEGMA grafted stripes were monitored separately. As seen in **Figure 8**, changing the stripe chemistry did not influence the overall freezing propagation mechanism of the patterned wettability surfaces: freezing events still onset and propagate at the hydrophilic stripe(s) first to further expand transversally onto the PP surface.

When analyzing the freezing mechanisms involved in the freezing of the patterned wettability surfaces (Figures 7, 8; and Figures S5, S6, and Video S3, Supporting Information), two separate freezing propagation rates were calculated for the two contrasting freezing propagation steps and modes: i) rapid freezing initiation and propagation along the hydrophilic stripes (**Figure 9**a,c), and ii) slower lateral freezing front propagation from the stripes into the more hydrophobic substrates (Figure 9b,d).

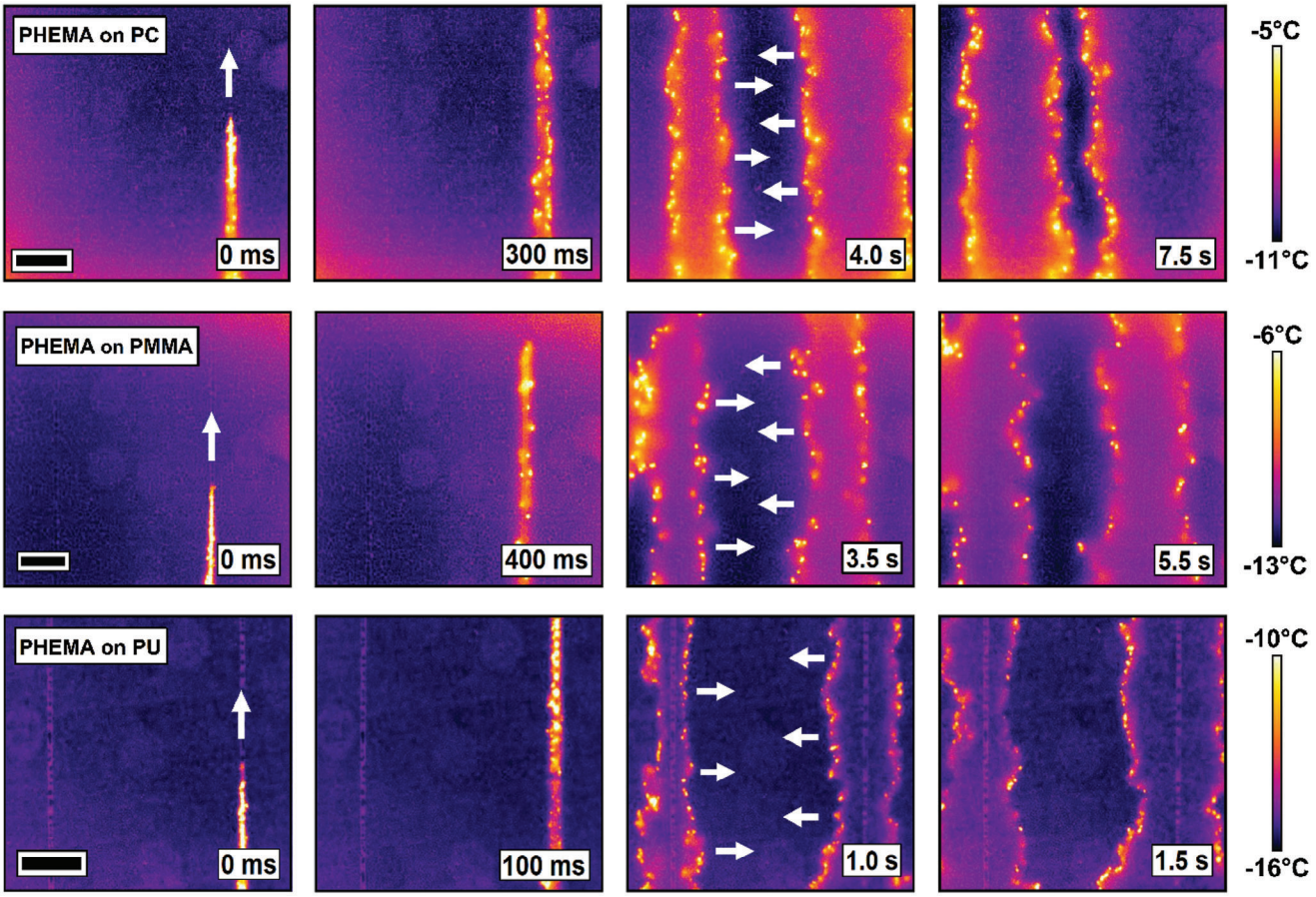

Figure 7. Thermal video snapshots showing freezing propagation in RH 50% on three different polymer substrates (PC, PMMA, PU) patterned with hydrophilic PHEMA stripes. The white arrows indicate the direction of the freezing propagation. The black scale bar equals 2 mm. Note the similar patterns but at different nucleation times and propagation rates.

When comparing Figures 6b and 9a, it becomes clear that the propagation mode and speed on the stripes (10 mm s^{-1}, Figure 9a) resemble those seen on the polymers homogeneously covered with PHEMA (20 mm s^{-1}, Figure 6b). A similar comparison can be made for the freezing propagation rates for the hydrophobic polymers (Figure 6a) and the lateral freezing propagation mode on the patterned surfaces perpendicular to the stripes (Figure 9b). In this case, we report an order of magnitude faster propagation rates on the hydrophobic surfaces when the surfaces are patterned with hydrophilic stripes.

An explanation to this difference can be found in the theory of ice-bridge kinetics based on Kinetic Monte Carlo simulations which predicted that the rate of ice-bridge formation increases with decreasing inter droplet distance, increasing temperature, or increasing surface wettability.[59] Since the experimental procedure did not change at any point, the influence of temperature, i.e., higher degree of supercooling cannot explain the observed faster propagation rates. Also, the wettability of the polymer substrates at areas that were covered during the UV exposure did not change after the grafting procedure, as shown in Figure S9 in the Supporting Information. Therefore, changes in both surface temperature and wettability of the substrates can be excluded, and the increased frost propagation rate is likely due to shorter distances between condensed water droplets.

On the patterned surfaces, the freezing events initiate on the hydrophilic stripes where the nucleation events are energetically more favorable and therefore happen earlier than on the more hydrophobic bare polymers. The earlier the initial nucleation event occurs, the less time the existing condensed water droplets have to grow in size and coalesce with each other. Droplet coalescing leads to longer inter-droplet distances since depressed vapor pressure over larger droplets promotes evaporation of its smaller neighbouring droplets.[34] Therefore, during an earlier nucleation event on the patterned surfaces, the condensed water droplets are smaller and closer together which accounts for the faster inter-droplet ice bridging rates.

In addition to the faster frost propagation rates in the patterned surfaces, the same linear dependency with the hysteresis contact angle (CAH) can be observed, i.e., connection of the lateral freezing propagation rate to the wettability of the polymeric substrate and the role of the MWL on local freezing propagation along the stripes. Earlier research measuring the thickness and continuity of MWLs with FTIR, AFM, thermal imaging, and X-ray reflectometry has shown a clear difference in the presence and state of MWL between hydrophilic and hydrophobic surfaces.[9,12,17] In

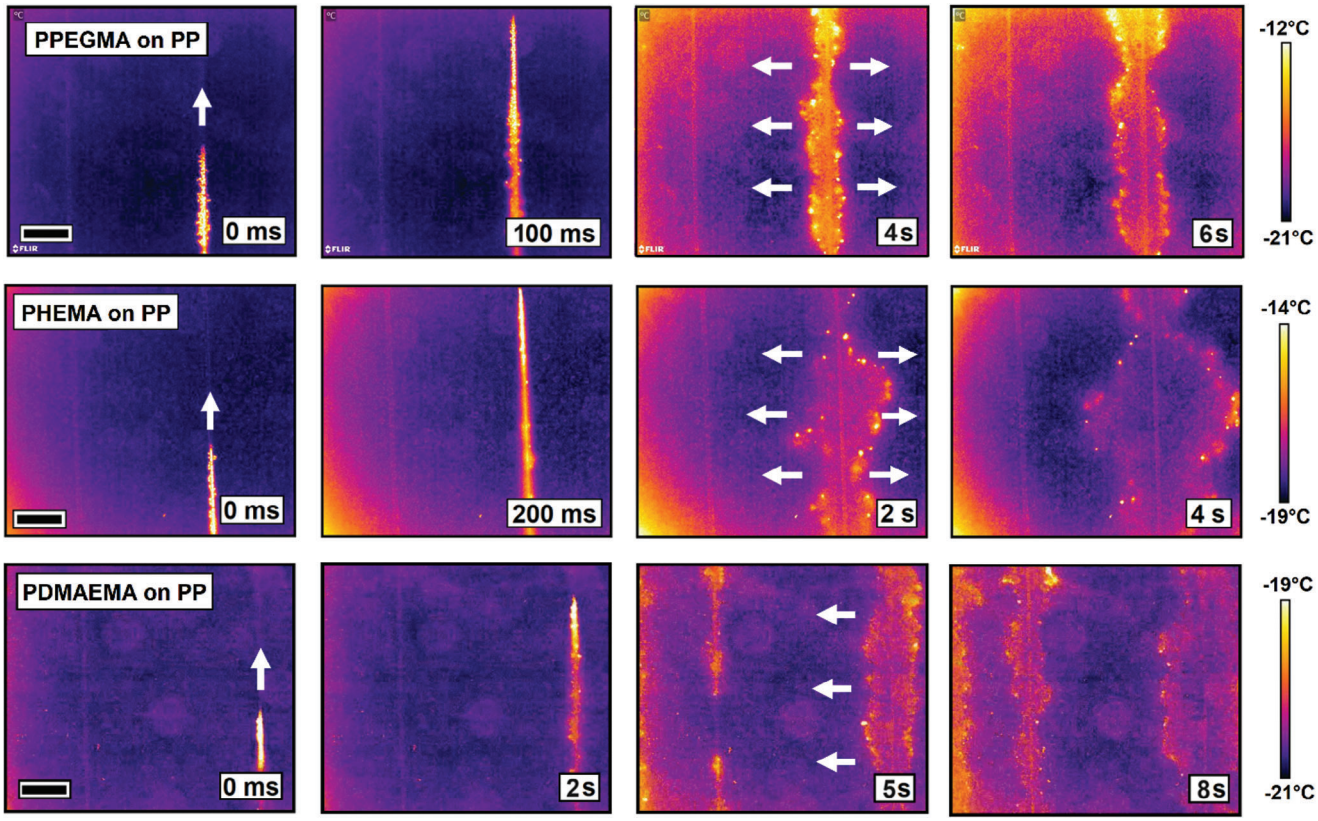

Figure 8. Thermal video snapshots showing freezing propagation in RH 50% on PP substrates patterned with PPEGMA, PHEMA, and PDMAEMA stripes. The white arrows indicate the direction of the freezing propagation. The scale bar equals 2 mm. Note the different nucleation times and propagation rates.

general, liquid-like MWL was found on all hydrophilic surfaces (WCA<80°) at ambient conditions, while the hydrophobic samples (WCA>80°) showed either no water adsorption at all or some water adsorption at surface defects depending on RH.

Considering the previous measurements on hydrophobic methyl-terminated monolayer surfaces,[9] it can be assumed that there is no water adsorption on the PP substrates at RT in 50% RH. On the other hand, the polymeric substrates grafted with hydrophilic polymers are expected to adsorb a continuous liquid-like MWL with a thickness >0.4 nm, as previously reported for hydrophilic COOH-terminated monolayers.[9] On the patterned surfaces, following the same logic, the hydrophilic stripes are expected to be covered with a continuous liquid-like MWL, whereas the surrounding bare polymeric substrate should have no MWL.

In our previous work,[17] we connected the presence and state of MWLs to different freezing propagation modes on surface-functionalized glass slides with varying wettability. On the dry hydrophobic surfaces in 50% RH, the freezing events propagated slowly (<0.05 mm s^{-1}) via ice-bridge formation. In the same environmental conditions, freezing events propagated rapidly (>2 mm s^{-1}) on very hydrophilic surfaces via a thin continuous liquid-like MWL. These same freezing propagation modes were detected here on the bare polymeric substrates (Figure 5) and the substrates grafted with hydrophilic polymers (Figure 5; and Figure S4, Supporting Information). The faster freezing propagation rates on the bare PU, PVC, and PMMA (0.1–1.0 mm s^{-1} in Figure 6a) are likely the result of some minor water adsorption at surface defects/higher surface roughness, as previously suggested for chloro-terminated monolayers and Teflon surfaces.[9,12]

As seen in Figure 9a, changing the chemistry of the hydrophilic stripes seems to also influence the rate of the rapid longitudinal freezing propagation on the patterned surfaces. The fast-freezing propagation mode along the stripes still corresponds to freezing via a continuous MWL, however, the propagation rate decreases with increasing wettability of the stripe. Similar to the bare polymer substrate, lowering the hydrophilicity of the polymer brush can result in less continuous MWL and a slower freezing propagation rate on the stripes.

The presence of the two distinctively different freezing propagation mechanisms on the patterned wettability surfaces (Figures 7 and 8) strongly indicates that localized wettability difference can induce localized variability in MWL which, moreover, can lead to localized variability in the freezing propagation speeds. As shown in **Figure 10**, the freezing events first propagate rapidly on the stripe through the continuous liquid-like MWL, after which the freezing propagation continues much more slowly on the dry polymeric substrate via ice-bridge formation being this process faster at higher hysteresis values of the hydrophobic substrate. This is attributed to the lower receding contact angles measured for the samples with the highest hysteresis which arguably contribute to a faster propagation of the MWL from the

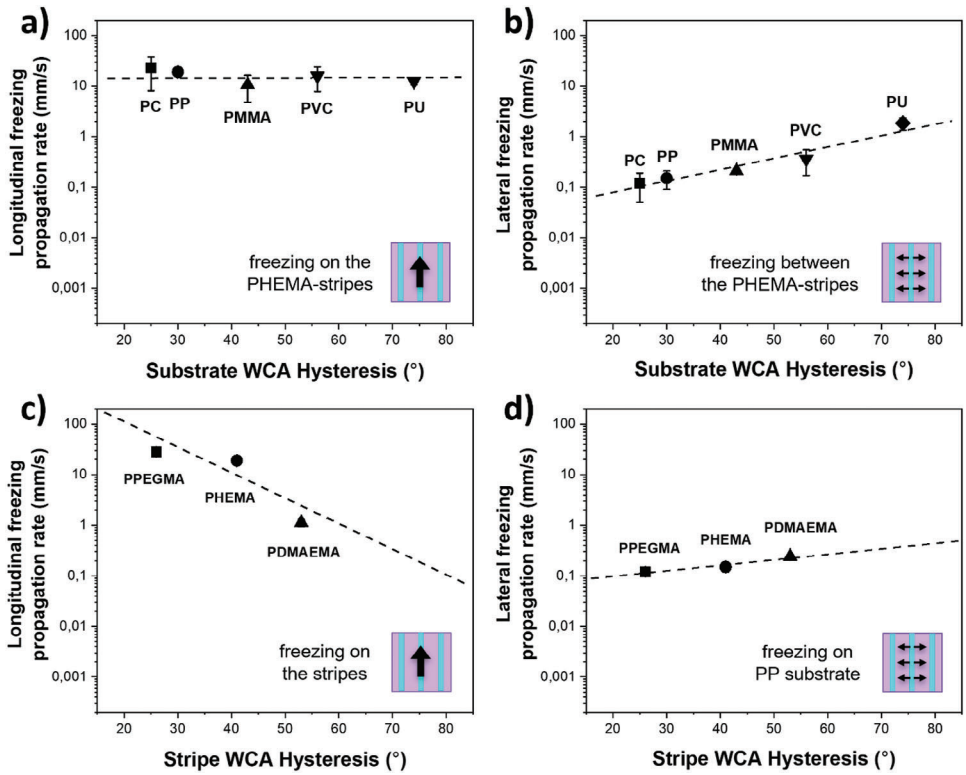

Figure 9. Freezing propagation rates on the patterned surfaces with PHEMA stripes and varying wettability of the hydrophobic substrate a,b), and the PP substrates with varying wettability of the hydrophilic stripes c,d). The propagation rates were calculated separately for the freezing events propagating longitudinally along the hydrophilic stripes a,c) and for the freezing events propagating laterally from the stripes onto the substrate b,d).

hydrophilic regions, hence accelerating the propagation rate in one order of magnitude with respect to the bare (slightly)hydrophobic polymers (Figure 6a vs 9b).

3. Conclusions

In this work, a set of five slightly hydrophobic polymers (PP, PU, PVC, PMMA, PC) were surface-modified to create stripped hydrophilic patterns on hydrophobic surfaces using SI-ATRP. This allowed studying the effect of pattern and substrate wettability local differences on surface freezing propagation mechanism. The condensation frost onset and propagation rate and mode were monitored in a high supersaturation environment ($S > 6.5$) using high-resolution thermal imaging. Local wettability differences on the polymeric substrates grafted with hydrophilic stripes were linked to local variations in the presence and state of MWL: the presence of localized liquid-like MWL was related to the fast-freezing events on the hydrophilic stripes and to the acceleration of the freezing propagation rate across the more hydrophobic substrate for the studied patterns and environmental conditions. A linear relation between inter-droplet ice propagation rate and CAH was found for the hydrophobic surfaces revealing propagation rates one order of magnitude faster than those reported for ice-droplet freezing. In the future, these insights could be used to develop new ice-controlling surfaces based on the idea of local ice nucleation and propagation control. The findings here reported may also contribute to a better understanding of freezing mechanisms on surfaces with defects and impurities with varying molecular water layers.

4. Experimental Section

Reagents and Materials: PC, PP, PMMA, PU, and PVC were used as substrates in this work. PU substrates were prepared as described elsewhere.[60] All other polymer substrates (PC, PP, PMMA, and PVC) used in this work were purchased from S-Polytec GmbH. Glycidyl methacrylate (GMA, 97%), 2-hydroxyethyl methacrylate (HEMA, 97%), 2-(dimethylamino)ethyl methacrylate (DMAEMA, 98%), 4-cyano-4-(phenylcarbonothioylthio)pentanoic acid (CTA), 2,2′-azobis(isobutyronitrile) (AIBN, 98%), sodium azide (NaN_3, 99.5%), triethylamine (TEA, 99.7%), copper(I)bromide (CuBr, 98%), copper(II) bromide ($CuBr_2$, 99%), and 2-bromoisobutyrylbromide (BIBB, 98%) were purchased from Merck Sigma. Poly(ethylene glycol) methacrylate (PEGMA, M_n = 500), and *N*,*N*,*N*0,*N*0,*N*0-Pentamethyldiethylenetriamine (PMDETA, 99%) were purchased from TCI Europe. All solvents used in this study were of analytical grade and used as received.

Synthesis of PGMA Backbone: Poly(glycidyl methacrylate) (PGMA) was synthesized via reversible-addition-fragmentation chain transfer (RAFT) polymerization using 4-cyano-4-(phenylcarbonothioylthio)pentanoic acid (CTA) as a chain transfer agent.[40] First, GMA (3 mL, 23 mmol), AIBN (9.27 mg, 0.056 mmol), and CTA (63.1 mg, 0.23 mmol) were transferred into a 50 mL round-bottomed reaction flask using 1,4-dioxane (2 mL) as a solvent.[41] The molar feed ratio of the reagents [GMA]:[AIBN]:[CTA] was 100:0.25:1. After oxygen was removed from the reaction flask by 5 freeze-pump-thaw cycles, the reaction was carried out under a nitrogen atmosphere at 65 °C while stirring at 250 rpm. The reaction was stopped after

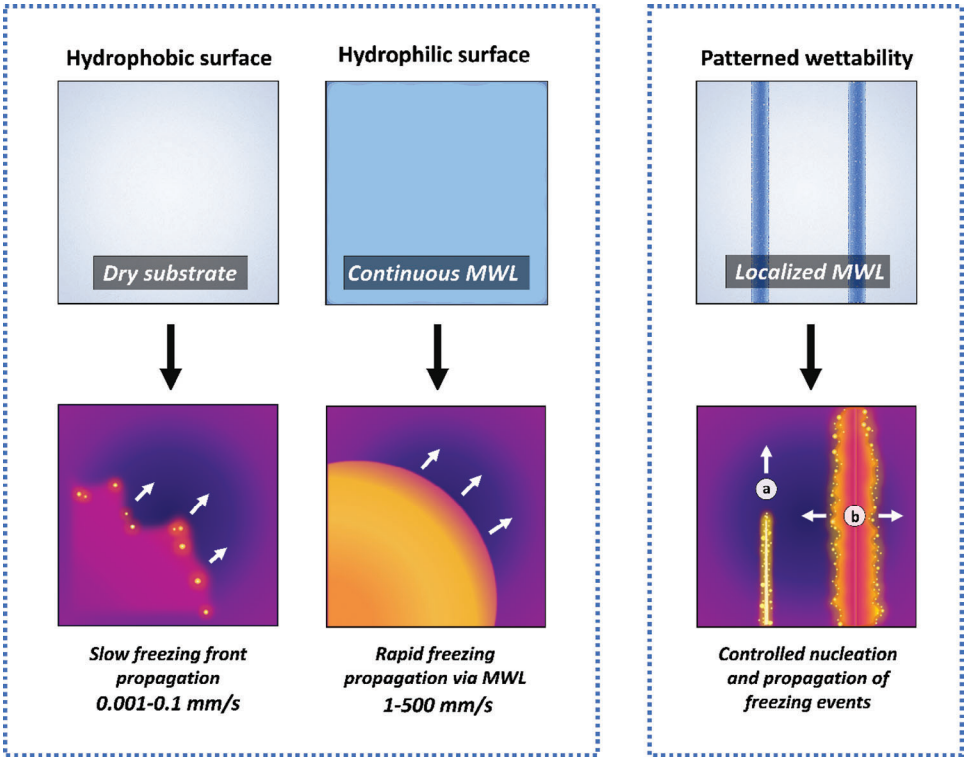

Figure 10. Illustration representing how local variations in the state of MWL can be used to control nucleation and propagation of freezing events on patterned wettability surfaces. On hydrophobic surfaces with hydrophilic stripes, the initial freezing events nucleate on the hydrophilic areas and propagate rapidly along the hydrophilic stripes a) via liquid-like MWL. After local hydrophilic stripes are frozen, the freezing event continues to propagate laterally on the hydrophobic areas from the stripes at a significantly lower propagation rate b).

24 h by opening the reaction flask to air. To decrease the viscosity of the reaction mixture, 5 mL of THF was added into the flask, after which, the product was extracted from the reaction mixture by dropwise addition to 300 mL of cold methanol under vigorous stirring. The mixture was filtered under reduced pressure, and the filtered product was redissolved to THF to purify it with two reprecipitations.[42] The purified pink-colored PGMA was dried overnight under reduced pressure (5 mbar) at RT. Based on the mass of the purified and dried PGMA, the yield of the product was calculated as 79%. All synthesis steps were monitored by FTIR and ^{1}H-NMR (Figures S2, S3 in the Supporting Information).

Introduction of Azide Groups onto PGMA (PAzMA): An azide functionality was introduced to the polymer chain via a ring-opening reaction between the epoxide groups of the PGMA and sodium azide (NaN_3).[43–44] Dried PGMA (1.5 g), sodium azide (2.06 g), and ammonium chloride (1.7 g) were dissolved into DMF (25 mL) in a 100 mL round-bottomed reaction flask. The reaction was carried out in a 50 °C oil bath while stirring at 250 rpm for 24 h. Afterward, the product was extracted from the reaction mixture by dropwise addition to 400 mL of cold deionized water under vigorous stirring. The mixture was filtered under reduced pressure, and the filtered product was redissolved to THF to purify it with two reprecipitations. The purified colorless PAzMA was dried overnight under reduced pressure (5 mbar) at RT. The yield of the product was calculated as 92%.

Introduction of Bromide Groups onto PAzMA (PAzBrMA): A bromide functionality was added to the polymer chain via an esterification reaction between the OH-groups of the PAzMA and 2-bromoisobutyrylbromide (BIBB).[44] Dried PAzMA (1.0 g) and TEA (1.5 mL) were first dissolved into THF (40 mL) in a 250 mL three-necked round-bottomed reaction flask. The reaction flask was kept in an ice bath while 2.5 mL of BIBB in 20 mL of THF was added dropwise into the reaction mixture over a 45-min period in continuous magnetic stirring. The reaction was allowed to proceed at room temperature for 24 h, after which TEA hydrobromide salt was removed from the reaction mixture by filtering under reduced pressure. Before precipitation, the filtrate was concentrated to <10 mL by removing most of the THF with a rotary evaporator. Finally, the product was extracted from the concentrate by dropwise addition to 400 mL of cold deionized water under vigorous stirring. The mixture was filtered under reduced pressure, and the filtered product was redissolved to THF to purify it with two reprecipitations. The purified slightly-orange-colored PAzBrMA was dried overnight under reduced pressure (5 mbar) at RT. The yield of the product was calculated as 93%.

Surface Functionalization with PAzBrMA: The polymeric substrates (20 × 20 × 3 mm) were spin-coated with PAzBrMA solution (60 µL of 10 mg mL^{-1} in ethanol-acetone 6:1 mixture) at 1000 rpm for 20 s. Right after spin coating, the panels were exposed to a UV-light lamp (<400 nm, 5 min) to initiate the covalent attachment of the PAzBrMA macroinitiator through the azide group. After UV exposure, the samples were washed with an ethanol-acetone (6:1) mixture solution to remove the unreacted polymer chains from the sample surfaces.[45] For the preparation of the patterned surfaces, a suitably patterned UV mask was placed on top of the substrates during the UV-light exposure, followed by the same washing procedure. The UV masks were created by laser-cutting predesigned patterns (100 µm wide stripes with 0.5 mm distance between stripes) into a 0.8 mm thin polyester sheet.

Grafting of Hydrophilic Monomers on PAzBrMA-Modified Polymer Substrates: To modify the surface chemistry of the Br-functionalized surfaces, SI-ATRP of three hydrophilic monomers (HEMA, PEGMA, and DMAEMA) was carried out in a 50 mL round-bottom flask.[45–46] All reagents and their amounts in the three different polymerizations can be found in Table S1 in the Supporting Information. For example, HEMA (4 mL), CuBr2 (14.7 mg), PMDETA (69 µL), and four of the PAzBrMA-functionalized surfaces (2 × 2 cm^2) were placed in 4 mL of deionized water. After degassing the mixture

with nitrogen for 30 min, CuBr (47.3 mg) was added to the mixture. The polymerization was terminated after stirring at RT for 4 h by opening the reaction flask to air. Finally, the samples were extracted from the flask and washed in aqueous ethylenediaminetetraacetic acid disodium salt (EDTA) solution, followed by rinsing with deionized water.

Water Contact Angle Measurements: Water contact angles (WCAs) of the bare and grafted polymer surfaces were determined using a KSV CAM 200 optical contact angle goniometer. Static, advancing, and receding water contact angles were recorded using the sessile and needle-in-the-sessile-drop methods. All measurements were repeated three times for each sample. For advancing (A-WCA) and receding (R-WCA) angles the initial volume of the drop (3 µL) was first increased with a pumping speed of 15 µL s^{-1} until a maximum droplet size of 15 µL. Then the volume of the droplet was decreased from 15 µL back to 3 µL using the same pumping speed of 15 µL s^{-1}. All WCA measurements were carried out at an ambient temperature of 21 °C ±2 and relative humidity of 40% ±5.

Surface Imaging: The polymeric substrates were imaged before and after the surface functionalization using Laser Scanning Confocal Microscopy (Keyence VK-X1000) and micro-FTIR (PerkinElmer Spotlight 400). The 3D Laser Scanning Confocal images were further analyzed to determine area roughness values (S_a) for the sample surfaces.

Measuring and Quantifying Freezing Events with Thermal Imaging: Freezing events on the substrates were monitored using a thermal imaging setup described in the previous work.[17] The cooling system of the setup was modified with a liquid-cooled thermoelectric cold plate (102 × 102 mm, LHP-300CP, ThermoElectric Cooling America Corporation). A small acrylic environmental chamber (10 × 10 × 10 mm) was built to fit on top of the cooling system for humidity control during the experiments. The relative humidity was lowered with a flow of nitrogen gas and increased with a flow of humid air from a bubbler system. The temperature inside the chamber was monitored throughout the experiments as close to the sample surface as possible. After turning the cooling stage on at the beginning of each experiment, the in-chamber temperature dropped slowly from 21 to 4 °C.

Supporting Information

Supporting Information is available from the Wiley Online Library or from the author.

Acknowledgements

This project has received funding from the European Union's Horizon 2020 research programme under the Marie Skłodowska-Curie grant Agreement No 956703 (SURFICE project).

Conflict of Interest

The authors declare no conflict of interest.

Data Availability Statement

The data that support the findings of this study are available from the corresponding author upon reasonable request.

Keywords

anti-icing, condensation frosting, contrast wettability, controlled icing, interfacial water, patterned wettability, thermal imaging

Received: October 23, 2024
Revised: November 25, 2024
Published online: January 8, 2025

[1] Y. Lin, H. Chen, G. Wang, A. Liu, *Coatings* **2018**, *8*, 208.
[2] Y. Shen, X. Wu, J. Tao, C. Zhu, Y. Lai, Z. Chen, *Prog. Mater. Sci.* **2019**, *103*, 509.
[3] X. Huang, N. Tepylo, V. Pommier-Budinger, M. Budinger, E. Bonaccurso, P. Villedieu, *Prog. Aerosp. Sci.* **2019**, *105*, 74.
[4] G. Hernández Rodríguez, M. Fratschko, L. Stendardo, C. Antonini, R. Resel, A. M. Coclite, *ACS Appl. Mater. Interfaces* **2024**, *16*, 11901.
[5] G. Hernández Rodríguez, G. Gastaldo, L. Stendardo, Y. Rafik, J. Pothin, M. Budinger, C. Antonini, V. Pommier-Budinger, A. M. Coclite, *Adv. Eng. Mater.* **2024**, 2401532, https://doi.org/10.1002/adem.202401532.
[6] X. Zhou, Y. Sun, J. Liu, *Adv. Mater. Interfaces* **2021**, *8*, 2100327.
[7] Y. Liu, Y. Wu, S. Liu, F. Zhou, *ACS Mater. Lett.* **2022**, *4*, 246.
[8] J. Hu, X. D. Xiao, D. F. Ogletree, M. Salmeron, *Science* **1995**, *268*, 267.
[9] M. James, T. A. Darwish, S. Ciampi, S. O. Sylvester, Z. Zhang, A. Ng, J. J. Gooding, L. Hanleya, *Soft Matter* **2011**, *7*, 5309.
[10] T. K. Shimizu, S. Maier, A. Verdaguer, J. J. Velasco-Velez, M. Salmeron, *Prog. Surf. Sci.* **2018**, *93*, 87.
[11] C. Spagnoli, K. Loos, A. Ulman, M. K. Cowman, *J. Am. Chem. Soc.* **2003**, *125*, 7124.
[12] A. L. Sumner, E. Menke, Y. Dubrowski, J. Newberg, R. Penner, C. Hemminger, L. Wingen, T. Brauers, B. Finlayson-Pitts, *Phys. Chem. Chem. Phys.* **2004**, *6*, 604.
[13] D. B. Asay, S. H. Kim, *J. Phys. Chem. B* **2005**, *109*, 16760.
[14] H. Bluhm, T. Inoue, M. Salmeron, *Surf. Sci.* **2000**, *462*, L599.
[15] P. B. Miranda, L. Xu, Y. R. Shen, M. Salmeron, *Phys. Rev. Lett.* **1998**, *81*, 5876.
[16] S. Santos, A. Verdaguer, *Materials* **2016**, *9*, 182.
[17] M. J. Tavaststjerna, S. J. Picken, S. J. Garcia, *Langmuir* **2024**, *40*, 12888.
[18] R. P. Garrod, L. G. Harris, W. C. E. Schofield, J. McGettrick, L. J. Ward, D. O. H. Teare, J. P. S. Badyal, *Langmuir* **2007**, *23*, 689.
[19] K. K. Varanasi, M. Hsu, N. Bhate, W. Yang, T. Deng, *Appl. Phys. Lett.* **2009**, *95*, 094101.
[20] Z. W. Yu, F. F. Yun, Y. Q. Wang, L. Yao, S. Dou, K. S. Liu, L. Jiang, X. L. Wang, *Small* **2017**, *13*, 1701403.
[21] Z. Chen, Z. Zhang, *Water Sci. Technol.* **2020**, *82*, 207.
[22] H. Bai, L. Wang, J. Ju, R. Sun, Y. Zheng, L. Jiang, *Adv. Mater.* **2014**, *26*, 5025.
[23] T. Dimitriadis, L. Stendardo, I. Tagliaro, A. M. Coclite, C. Antonini, T. Maitra, *ACS Appl. Mater. Interfaces* **2023**, *15*, 27206.
[24] N. M. Oliveira, S. Vilabril, M. B. Oliveira, R. L. Reis, J. F. Mano, *Mater. Sci. Eng., C* **2019**, *97*, 851.
[25] Y. Segawa, K. Kinoshita, H. Kai, *Adv. Mater. Interfaces* **2023**, *10*, 2300340.
[26] C. Gao, L. Zhang, Y. Hou, Y. Zheng, *Adv. Mater.* **2023**, *35*, 2304080.
[27] Y. Li, B.-F. Liu, X. Zhang, *Mater. Today* **2021**, *51*, 273.
[28] L. Mishchenko, M. Khan, J. Aizenberg, B. D. Hatton, *Adv. Funct. Mater.* **2013**, *23*, 4577.
[29] A. Kirillova, L. Ionov, I. V. Roisman, A. Synytska, *Chem. Mater.* **2016**, *28*, 6995.
[30] J. Boreyko, R. Hansen, K. Murphy, S. Nath, S. T. Retterer, C. P. Collier, *Sci. Rep.* **2016**, *6*, 19131.
[31] J. L. O'Brien, S. F. Ahmadi, K. C. Failor, C. E. Bisbano, M. D. Mulroe, S. Nath, B. A. Vinatzer, J. B. Boreyko, *Appl. Phys. Lett.* **2018**, *113*, 153701.
[32] Y. Jin, C. Wu, Y. Yang, J. Wu, Z. He, J. Wang, *ACS Nano* **2020**, *14*, 5000.
[33] C.-W. Lo, V. Sahoo, M.-C. Lu, *ACS Nano* **2017**, *11*, 2665.
[34] S. Nath, J. B. Boreyko, *Langmuir* **2016**, *32*, 8350.
[35] S. Nath, C. E. Bisbano, P. Yue, J. B. Boreyko, *J. Fluid Mech.* **2018**, *853*, 601.
[36] R. Williams, J. Blanc, *J. Chem. Phys.* **1981**, *74*, 4675.
[37] J. Guadarrama-Cetina, R. D. Narhe, D. Beysens, W. González-Viñas, *Phys. Rev. E: Stat., Nonlinear, Soft Matter Phys.* **2014**, *89*, 012402.
[38] J. Guadarrama, A. Mongruel, W. González-Viñas, D. Beysens, *Europhys. Lett.* **2015**, *110*, 56002.

[39] X. Sun, V. G. Damle, A. Uppal, R. Linder, S. Chandrashekar, A. R. Mohan, K. Rykaczewski, *Langmuir* **2015**, *31*, 13743.
[40] J. Zhu, D. Zhou, X. Zhu, G. Chen, *J. Polym. Sci. A Polym. Chem.* **2004**, *42*, 2558.
[41] C. S. Gudipati, M. B. H. Tan, H. Hussain, Y. Liu, C. He, T. P. Davis, *Macromol. Rapid Commun.* **2008**, *29*, 1902.
[42] Z. Cheng, X. Zhu, G. D. Fu, E. T. Kang, K. G. Neoh, *Macromolecules* **2005**, *38*, 7187.
[43] H. Thankappan, M. Semsarilar, S. Li, Y. Chang, D. Bouyer, D. Quemener, *Molecules* **2020**, *25*, 4774.
[44] C. Zhao, D. Wu, X. Lian, Y. Zhang, X. Song, H. Zhao, *J. Phys. Chem. B* **2010**, *114*, 6300.
[45] D. Pranantyo, L. Xu, K.-G. Neoh, E.-T. Kang, W. Yang, S. Teo, *J. Mater. Chem. B* **2014**, *2*, 398.
[46] G. Panzarasa, S. Aghion, G. Marra, A. Wagner, M. O. Liedke, M. Elsayed, R. Krause-Rehberg, R. Ferragut, G. Consolati, *Macromolecules* **2017**, *50*, 5574.
[47] Y. Zhang, H. He, C. Gao, *Macromolecules* **2008**, *41*, 9581.
[48] S. Nath, S. F. Ahmadi, J. B. Boreyko, *Soft Matter* **2020**, *16*, 1156.
[49] J. Guadarrama, A. Mongruel, W. González-Viñas, D. Beysens, *Europhys. Lett.* **2013**, *101*, 16009.
[50] D. Paulovics, C. Raufaste, T. Frisch, C. Claudet, F. Celestini, *Langmuir* **2022**, *38*, 2972.
[51] Y. Zhao, C. Yang, *Appl. Therm. Eng.* **2017**, *121*, 136.
[52] Y. Zhao, R. Wang, C. Yang, *Int. J. Heat Mass Transfer* **2017**, *108*, 1048.
[53] Y. Zhao, C. Yang, *Appl. Phys. Lett.* **2016**, *108*, 061605.
[54] M. R. Haque, S. R. Das, A. R. Betz, *Appl. Therm. Eng.* **2019**, *160*, 113987.
[55] M. Schremb, I. Roisman, C. Tropea, *J. Fluid Mech.* **2018**, *835*, 1087.
[56] J. E. Castillo, Y. Huang, Z. Pan, J. A. Weibel, *Int. J. Heat Mass Transfer* **2021**, *164*, 120608.
[57] Z. Meng, P. Zhang, *Int. J. Heat Mass Transfer* **2020**, *152*, 119468.
[58] M. Schremb, I. Roisman, C. Tropea, *13th Triennial International Conference on Liquid Atomization and Spray Systems*, Tainan, Taiwan, August 23–27, 2015.
[59] S. Curiotto, D. Paulovics, C. Raufaste, F. Celestini, T. Frisch, F. Leroy, F. Cheynis, P. Müller, *Langmuir* **2023**, *39*, 579.
[60] V. Montano, M. Wempe, S. Does, J. Bijleveld, S. Zwaag, S. García, *Macromolecules* **2019**, *52*, 8067.